Temperature influence on water transport in hardened cement pastes

Emeline Drouet, Stéphane Poyet, Jean-Michel Torrenti

Temperature influence on water transport

in hardened cement pastes.

Emeline DROUET [a], Stéphane POYET [a,*], Jean-Michel TORRENTI [b]

[a] CEA, DEN, DPC, SECR, Laboratoire d'Etude du Comportement des Bétons et des Argiles, F-91191 Gif sur Yvette Cedex, France.

[b] Université Paris-Est, IFSTTAR, Département Matériaux & Structures, 14-52 boulevard Newton, F-77447 Marne la Vallée cedex 2, France.

Abstract

Describing water transport in concrete is an important issue for the durability assessment of radioactive waste management reinforced concrete structures. Due to the waste thermal output such structures would be submitted to moderate temperatures (up to 80°C). We have then studied the influence of temperature on water transport within hardened cement pastes of four different formulations. Using a simplified approach (describing only the permeation of liquid water) we characterized the properties needed to describe water transport (up to 80°C) using dedicated experiments. For each hardened cement paste the results are presented and discussed.

Keywords: Waste management (E) – Cement paste (D) – Drying (A) – Temperature (A) - Permeability (C).

1. Introduction

Water plays a very important role in concrete structures durability. This fact is well illustrated by the results of Tuutti [1] which relate the variations of the corrosion current of steel embedded in a carbonated mortar as a function of the external relative humidity (RH). In a more general way water is necessary for the chemical reactions to occur (in solution) and presents a significant impact on concrete transport properties. The durability assessment of concrete structures thus necessitates an accurate description of water transport all along service life. Among the data needed to compute water flow in unsaturated conditions, the water sorption isotherm and permeability are the most important (see part 2). In the field of radioactive waste management, the concrete structures and containers would also have to cope with heating due to the waste thermal output (the maximal temperature to be reached is 80°C).

It has been known for long that water transport is strongly influenced by temperature. Experiments performed on cementitious materials have shown that the higher the temperature, the faster the water transport [2-9]. Several authors used the diffusion equation to describe isothermal drying experiments. In so doing, the resulting moisture diffusivity D was found to increase with temperature. Glover and Raask [4] showed the moisture diffusivity of a Portland cement paste (water-to-cement ratio w/c = 0.28) was multiplied by 11 to 15 between 30 and 70°C whereas Wong et al. [7] obtained a factor 6 to 8 between 20 and 40°C for three concretes (Portland cement, w/c = 0.4, 0.5 and 0.6). In the same way Powers [5] measured the permeability of Portland cement pastes (w/c from 0.5 to 0.8) between 0 and 27°C using water. The resulting hydraulic conductivity (that depends on water viscosity, in m/s) was found to increase by a factor 3. Hughes et al. [2] and Hancox [3] dried Portland cement paste samples (w/c = 0.3 and 0.5) at temperatures ranging from 21 to 95°C. The diffusivity increase with temperature was found to follow Arrhenius' equation. The mean activation energy was 43 kJ/mol (10.2 kcal/g/mol).

40 It must be mentioned that smaller increase in water transport properties were obtained in recent

41 studies. Jooss and Reinhardt [9] measured water permeability and diffusivity of several different

42 cementitious materials (using water permeametry and cup method). They found that permeability and

43 diffusivity were only increased by 18-92% and 18-41% respectively between 20 and 80°C. Černy et al. [8]

44 used the so-called PCK method (similar to an imbibition test) to estimate the moisture diffusivity of two

45 concrete used for nuclear power plants containment building in France and Czech Republic. The values

46 obtained at 80°C were greater than the ones obtained at 5°C by a factor 2.0-2.5.

47 Temperature is also known to affect the water retention properties of cementitious materials [6, 10-15].

48 A temperature increase leads to the reduction of the amount of water retained at equilibrium with a

49 given RH: the greater the temperature increase, the more the reduction. For instance for a high-

50 performance concrete kept at 60% RH, increasing temperature from 30 to 80°C led to the reduction of

51 the water content (by mass) at equilibrium from 3% to about 1% [13]. The isotherm shape is also

52 modified; the water content reduction is not constant over the RH-range. It depends on the temperature

53 increase. Another important point is the absence of temperature threshold: any change in temperature

54 is expected to impact the water retention curve.

55 The influence of temperature is generally attributed to the variation of water physical properties (density

56 and surface tension) [16] as well as the coarsening of the pore structure in relation to ettringite

57 dissolution and C-S-H alteration [14]. It was however suggested recently that another phenomenon

58 might be at work [13]. A temperature change at a constant RH leads to the shift of equilibrium between

59 the adsorbed phase and water vapor. Since adsorption is an exothermic process, a temperature increase

60 shifts the equilibrium towards the endothermic reaction (that is to say desorption). Consequently water

61 is released. A simple tool was then proposed to describe this so-called "thermal desorption" [17]. It is

62 based on Clausius-Clapeyron equation [18]:

63
$$q_{st}(w) = -R \left.\frac{\partial \ln(p_v)}{\partial\left(\frac{1}{T}\right)}\right|_w \qquad (1)$$

64   where:

65   • R is the universal gas constant (8.3145 J/mol/K);

66   • p_v vapor pressure (Pa) at equilibrium with the water content w;

67   • T absolute temperature (K);

68   • q_{st} isosteric energy (J/mol).

69   q_{st} corresponds to the amount of heat involved in the adsorption process (J/mol). Note that in eq. (1) the

70   derivation operation must be carried out for a constant amount of adsorbed water w. The isosteric

71   energy q_{st} can be obtained using two isotherms at two distinct temperatures. Once q_{st} is known, the

72   water retention curve for any arbitrary temperature T can be easily estimated using:

73
$$h(w,T) = h(w,T_0)\frac{p_{vs}(T_0)}{p_{vs}(T)} \exp\left[q_{st}(w)\frac{T-T_0}{RTT_0}\right] \qquad (2)$$

74   where:

75   • $p_{vs}(T)$ is the vapor pressure at saturation (Pa) for the absolute temperature T;

76   • $h(w,T)$ relative humidity at equilibrium with the water content w at the absolute temperature T.

77   This simple model was found to satisfactorily reproduce the temperature-induced evolution of concrete

78   water retention curve [13, 17]. This model implicitly assumes that the shift of equilibrium is the only

79   mechanism at work and that the microstructure modifications can be neglected.

80   For the description of unsaturated water transport, the intrinsic permeability is commonly evaluated

81   through inverse analysis [19-22]: the temperature-induced modifications of the water retention curve

82   described above are then expected to have a significant influence on the permeability assessment [23].

83   The main objective of this study was to assess the influence of temperature on unsaturated permeability.

4

84 With regards to Andra's (the French agency for radioactive waste management) requirements in the

85 context of nuclear waste storage, we have designed an experimental campaign to acquire all the data

86 needed to describe unsaturated water transport using a simplified model (see section 2) and

87 cementitious materials of interest. The results do constitute a unique and consistent dataset.

2. Background

89 Water transport within porous media involves three different motions: (1) permeation of the liquid

90 water; (2) permeation of the gaseous phase (water vapor + dry air) and (3) diffusion of water vapor

91 within the gaseous phase. The neat description of these phenomena leads to three coupled differential

92 equations [20, 21, 24-27]. The major drawback of such an approach is the very large number of input

93 data that are difficult to acquire experimentally.

94 From a practical point of view, water transport can be profitably described in a simplified way using a

95 single equation accounting for liquid permeation only. The others motions (permeation of the gaseous

96 phase and water vapor diffusion) are neglected. This assumption was found to be valid for a hardened

97 cement paste (w/c = 0.35) with a permeability equal to 1.0×10^{-21} m^2 [20]. In a recent study Thiery et al.

98 [28, 29] estimated the respective contribution of each motion to the overall water flow. They showed

99 that the assumption validity domain depends on the material properties and especially on permeability.

100 For a high-performance concrete (w/c = 0.27) with low permeability (2×10^{-22} m^2) the assumption is valid

101 between RH=20% and 100% whereas it is only valid between RH=65% and 100% for a low-strength

102 concrete (w/c = 0.84) with high permeability (4×10^{-19} m^2).

103 The liquid water flow rate is given by the extension of Darcy's law for incompressible unsaturated media

104 [30]:

105
$$j_w = -\rho \frac{K}{\eta} k_r \text{grad}(P),$$
(3)

106 In which:

107 • η is the water viscosity [Pa s];

108 • ρ water density [kg/m^3];

109 • K intrinsic permeability [m^2];

110 • k_r relative permeability to water [without unit];

111 • P water pressure [Pa].

112 In unsaturated conditions the water pressure presents negative values $P \in$]-∞ ; 0]. It is evaluated using

113 Kelvin-Laplace equation:

114
$$P = -\rho \frac{RT}{M} \ln(h),$$
(4)

115 where M is the water molar mass [0.018 kg/mol].

116 The mass conservation equation writes:

117
$$\frac{\partial}{\partial t}(\rho \emptyset S) = -\text{div}\left(j_w\right) = -\text{div}\left[-\rho K \frac{k_r}{\eta} \text{grad}(P)\right],$$
(5)

118 In which

119 • S is the saturation index [without unit], it characterizes how pores are filled (by volume) with

120 liquid water. It ranges between 0 (dry state) and 1 (saturated state).

121 • $\emptyset$ is the concrete porosity [volume per volume, without unit].

122 In isothermal conditions (as this is the case in this study, see after) and assuming that water is

123 incompressible and that water flow is the only phenomenon at work (absence of dissolution or

124 precipitation), ρ and $\emptyset$ can be considered as constants. The following equation is obtained:

125
$$\emptyset \frac{\partial S}{\partial t} = \text{div}\left[K\frac{k}{\eta}\text{grad}(P)\right]$$
(6)

126   Assuming that a differentiable function exists between water saturation S and pressure P one can obtain:

127
$$\emptyset \left(\frac{\partial S}{\partial P}\right)\frac{\partial P}{\partial t} = \text{div}\left[K\frac{k}{\eta}\text{grad}(P)\right]$$
(7)

128   This simple equation allows the water transport description within the cementitious materials knowing

129   only four their properties, namely: the porosity $\emptyset$, the derivative of the capillary pressure function, the

130   intrinsic and relative permeability K and k_r. Following Savage and Janssen [31] the water retention curve

131   is almost described using the equation proposed by van Genuchten [32]:

132
$$S = \left[1 + \left(\frac{|P|}{P_0}\right)^{\frac{1}{1-m}}\right]^{-m}$$
(8)

133   where P_0 and m are two positive parameters: m (usually around 0.5) [without unit] whereas P_0 is

134   equivalent to a pressure [several tenths of MPa]. The use of Mualem's model [33] together with eq. (8)

135   allows deriving an analytical expression for the relative permeability k_r (the value of the parameters m

136   and P_0 are the same as above):

137
$$k_r = \sqrt{S}\left[1 - \left(1 - S^{\frac{1}{m}}\right)^m\right]^2 = \left[1 + \left(\frac{|P|}{P_0}\right)^{\frac{1}{1-m}}\right]^{-\frac{m}{2}}\left\{1 - \left(\frac{|P|}{P_0}\right)^{\frac{1}{1-m}}\left[1 + \left(\frac{|P|}{P_0}\right)^{\frac{1}{1-m}}\right]^{-m}\right\}^2$$
(9)

138   The left-hand term $\left(\frac{\partial S}{\partial P}\right)$ of equation (7) is given by:

139
$$\left(\frac{\partial S}{\partial P}\right) = \frac{m}{(m-1)P_0}\left(\frac{|P|}{P_0}\right)^{\frac{1}{1-m}}\left[1 + \left(\frac{|P|}{P_0}\right)^{\frac{1}{1-m}}\right]^{-1-m}$$
(10)

3. Methods

3.1. Materials

We used hardened cement pastes prepared using four different binders that were selected for their

potential interest for radioactive waste management in France:

- The CEM I 52.5 R CE PM-ES-CP2 (according to the European standard EN-206) from Val

  d'Azergues factory (France, Lafarge). This ordinary Portland cement (OPC) was selected by Andra

  (the French Agency for radioactive waste management) as a reference cement for the study of

  concrete structures and waste packages.

- The CEM II/B-LL 42.5 N CE CP2 from Le Teil factory (France, Lafarge). This cement (OPC + 25%

  limestone filler) was selected because it was used for the realization of a scale-one subsurface

  storage structure mockup (Galatée) [34-36].

- The CEM V/A (S-V) 42.5 N CE PM-ES-CP1 from Airvault factory (Calcia, France). This cement was

  selected by Andra as a reference binder for concrete packages.

- A low-alkanity ternary mix of CEM I/OPC (37.5%), silica fume (32.5%) and fly ash (35%). The

  cement used in this mix was provided by Lafarge, Le Teil factory, France (CEM I 52.5 N CE PM-

  ES). The silica fume and fly ash were provided by Condensil (S 95 DM) and Calcia respectively.

  This mix composition was designed in the field of geological disposal by [37, 38] to mitigate the

  heat emitted during hydration and limit the chemical interaction between clay minerals and

  concrete parts (alkaline plume) which could impair clay physical and chemical properties.

A unique water-to-binder ratio (w/b) was used to enable comparison between the four pastes. We chose

w/b = 0.40 because it allowed the CEM I paste to be representative of the concrete studied in [13]. The

resulting hardened cement paste is the same as the one embedding the concrete aggregates. For this

162   purpose, the paste water to binder ratio w/b was adjusted to account for the water brought by the

163   superplasticizer and absorbed by the aggregates. Moreover this value appeared to yield good properties

164   of each fresh paste (good workability, neither visible segregation nor bleeding). The composition of each

165   paste is given in Table 1.

Table 1. Composition of the pastes.

Compound	CEM I	CEM II	CEM V	Low-pH	Unit
OPC	1396	1023	759	468	g/L of paste
Calcareous filler	-	341	-	-	g/L of paste
Slag	-	-	298	-	g/L of paste
Fly ash	-	-	298	377	g/L of paste
Silica fume	-	-	-	405	g/L of paste
Water	558	545	542	500	g/L of paste
Superplasticizer	-	-	-	12.5	g/L of paste

168   The four pastes were prepared in the laboratory in ten consecutive batches (two liters each) spanning

169   over three days. Each specimen was cast in a cylindrical mold ($\varnothing$35 × H60 mm for water adsorption

170   experiments and $\varnothing$51 × H80 mm for permeability assessment experiments) which was then hermetically

171   closed and kept at 20°C for seven days before unmolding. All the specimens of the same formulation

172   were immersed in a special curing solution inside an air-tight chamber (to prevent carbonation) for three

173   months. The composition of the curing solution was adjusted to prevent calcium and alkalis leaching. For

174   the CEM I, CEM II and CEM V pastes we determined the curing solution composition by expression of the

175   pore solution [39] and analysis using ionic chromatography (Table 2). The samples used for extraction

176   were kept three months in sealed bags (rather than under water to prevent dilution of the alkalis).

177   Analysis of the solutions at the beginning and end of the cure showed limited change (Table 2).

Table 2. Composition of the interstitial solutions (in mmol/L) and pH of the curing solutions before and

after cure of the CEM I CEM II and CEM V pastes.

	CEM I				CEM II/B				CEM V/A			
	Na^+	K^+	Ca^{2+}	pH	Na^+	K^+	Ca^{2+}	pH	Na^+	K^+	Ca^{2+}	pH
Interstitial solution	47	452	2	13.7	91	94	1	13.2	87	533	2	13.7
Begining of cure	49	439	2	13.6	90	93	3	13.3	90	518	4	13.7
End of cure	54	455	3	13.6	96	95	5	13.2	85	474	2	13.7

180

181 The sodium content of the three cements is quite low (and especially in comparison to the potassium

182 content). This is a direct consequence of the cements composition, low in sodium (Table 3).

183 *Table 3. Chemical composition of the cements.*

	SiO_2	Al_2O_3	Fe_2O_3	CaO	MgO	SO_3	K_2O	Na_2O	MnO	TiO_2	LOI	INS
CEM I	21.0	3.4	4.5	65.0	0.62	2.7	0.72	0.09	-	-	1.3	0.2
CEM II/B	18.0	3.5	1.7	62.6	0.85	2.97	0.16	0.15	-	-	9.4	1.2
CEM V/A	30.0	11.2	3.6	46.4	2.75	2.8	1.16	0.2	0.1	0.6	2.1	-

184

185 For the Low-pH which pore solution is known to exhibit great concentration variations in the first months

186 of hydration (portlandite is gradually consumed to precipitate new C-S-H: portlandite completely

187 disappears after two months) [38], a different approach was chosen. Several samples were reduced into

188 a rough powder and added to deionized water to generate the curing solution.

189 After the curing period, both ends (top and bottom) of each sample were sawn (using a diamond wire

190 saw with water) and discarded. This resulted in smaller cylinders (Ø35×H50 mm for water adsorption

191 experiments and Ø51×H60 mm for permeability assessment experiments) that were assumed to present

192 homogeneous properties versus height [40-42]. Because the specimens were kept under water for three

193 months after casting, full saturation at the cure end was assumed: no additional procedure was thus

194   used to ensure initial saturation (for instance saturation under vacuum). It was however verified on a few

195   samples that no water uptake was observed after 48 hours under water and vacuum.

3.2. Mineralogical composition

197   The portlandite content was measured using thermogravimetric analysis (TGA). Just after the cure, a

198   specimen was powdered in a CO_2-free glove box and 120 mg (± 1 mg) were placed in an automated TG

199   analyzer (Netzsch STA 409 PC). The temperature was increased at constant rate (10 °C/min) under dry

200   nitrogen flowrate (60 mL/min). The portlandite content was computed using the mass loss obtained

201   between 400 and 600°C.

202   The C-S-H concentration was estimated following the approach of Olson and Jennings [43] that relates

203   the amount of water adsorbed at 20% RH to the C-S-H content. It was then implicitly assumed that the

204   calcium-to-silicon (C/S) ratio of the C-S-H was equal to 1.7. We took advantage of the experimental water

205   retention curves to assess the water content at equilibrium at 20%. The model proposed by Pickett [44]

206   was fitted to the experimental results and used to compute the water content at 20% (see part 3.4.).

3.3. Porosity and microstructure

208   The specific gravity of the saturated materials d_s was measured using the buoyancy method following

209   current recommendations (French standard P18-459:2010): the saturated specimens were weighed

210   under water and in air (using a 1 mg accurate device). In air, the water in excess on the specimen surface

211   was removed using a wet cloth. The measurements were done in an air-conditioned room (20 ± 2°C).

212   The porosity to water Ø (by volume) was determined by oven-drying until constant weight; different

213   drying temperatures were used from 20°C to 105°C for comparison purposes. At 20°C and 50°C we used

214   silica gel as desiccant (RH ≈ 3%) whereas calcium chloride proved to be much more efficient at 80°C (RH

215   measured at 0.0% using capacitive hygrometer). No desiccant was used at 105°C (the RH decrease

216 induced by heating at 105°C is high enough). A different five-sample set was used for each configuration.

217 Due to the great number of sample-sets all the five specimens were weighed together; this explains why

218 there is no variability information in this case (no standard deviation).

219 The pore-size distribution was characterized using mercury intrusion porosimetry (MIP). Some specimens

220 were first kept a few months in sealed containers above silica gel (at 20°C and 50°C) or calcium chloride

221 (at 80°C) to remove most of the evaporable water. They were crushed into pieces (several millimeters

222 thick), freeze-dried using liquid nitrogen and eventually tested (up to 414 MPa). Three or four replicates

223 were tested for each experiment.

224 The specific surface area of each paste was assessed either directly by MIP or by post-processing the

225 experimental water desorption isotherms using the linear form of the BET model [45]:

226
$$\frac{h}{(1-h)w} = \frac{1}{C^B w_m^B} + \frac{C^B-1}{C^B w_m^B} h \tag{11}$$

227 where C^B and w_m^B are the two BET parameters. C^B is related to the energy of the first adsorbed layer and

228 w_m^B is the water content needed to complete a monomolecular layer. The BET linear form was used to

229 check the validity domain (for which the experimental points follow a straight line). The specific surface

230 area S_S was evaluated using the BET monolayer values w_m^B using [46]:

231
$$S_S = N_A \frac{A_w}{\rho V} w_m^B \tag{12}$$

232 where N_A is Avogadro's number ($N_A = 6.02 \times 10^{23}$ mol^{-1}); V is water molar volume ($V = 1.80 \times 10^{-5}$ m^3/mol at

233 20°C) and A_w is the surface area occupied by one water molecule on the sample surface. It was estimated

234 using [47, 48]:

235
$$A_w = 1.091 \left(\frac{M}{\rho N_A}\right)^{\frac{2}{3}} \tag{13}$$

3.4. Water retention curves

They were characterized in a classical way using the desiccator method [49] following the protocol used in [13]. Four cylinders (Ø35×H50 mm) of each formulation were put in a desiccator above a saturated salt solution for RH control (sixteen specimens were then introduced into the same desiccator). The specimen dimensions may seem big, but the low specific surface area of the specimens allowed us not to take any precaution against carbonation and to limit the potential impact of sawing (superficial cracking). The main disadvantage was the increase of the time needed to reach hygral equilibrium. We then determined the whole desorption isotherm for each paste by submitting different sets of specimens to different RHs (using different desiccators) simultaneously rather than submitting a unique set to decreasing RH steps. This was expected to induce some variability but it allowed reducing drastically the whole experiment duration.

This experiment was conducted at 20, 50 and 80°C. At 20°C, the desiccators were kept in an air-conditioned room (20°C ± 2°C) whereas ovens were used for the two other temperatures: three different ovens were used for 50°C and two for 80°C. At 50°C the regulation did not appear to be fully satisfactory: the temperature in the three ovens was found to be ranging from 50 to 60°C. This is believed to have induced some variability in the isotherm characterization. At 80°C, the temperature variability was far less than 1°C. The salt solutions used and the resulting RHs are reported in Table 4.

Table 4. Relative humidity as a function of temperature and saturated salt solution [50-54].

Saturated salt solutions		Temperature		
		20°C	50°C	80°C
Calcium chloride	$CaCl_2$	5%	3%	≈0%
Silica gel	SiO_2	3%	3%	≈10%
Lithium chloride	LiCl	11%	11%	11%
Magnesium chloride	$MgCl_2$	33%	31%	26%
Potassium carbonate	K_2CO_3	43%	-	-
Magnesium nitrate	$Mg(NO_3)_2$	54%	-	-

13

Sodium bromide	NaBr	59%	51%	51%
Urea	$CO(NH_2)_2$	-	62%	-
Ammonium nitrate	NH_4NO_3	63%	-	-
Potassium iodide	KI	70%	64%	61%
Sodium nitrate	$NaNO_3$	-	69%	65%
Sodium chloride	NaCl	-	74%	76%
Ammonium sulfate	$(NH_4)_2SO_4$	-	79%	-
Ammonium chloride	NH_4Cl	80%	-	-
Potassium chloride	KCl	-	-	80%
Potassium nitrate	KNO_3	-	85%	-
Sodium carbonate	Na_2CO_3	-	-	85%
Barium chloride	$BaCl_2$	90%	-	-
Sodium sulfate	Na_2SO_4	-	-	90%
Potassium sulfate	K_2SO_4	98%	96%	95%
Deionized water	H_2O	100%	100%	100%

254

255   Periodically we opened each desiccator, weighed each specimen-set (weighing each sample would have

256   been too much time-consuming) and computed the corresponding relative mass variation to monitor

257   sample drying:

$$\left(\frac{\Delta m}{m}\right)(t) = \frac{m(t) - m(t_0)}{m(t_0)} \qquad (14)$$

259   where $m(t)$ is the mass for the time t and the mass for the time t (t_0 corresponds to the experiment

260   beginning). The difference from equilibrium was characterized using the following indicator ε which is an

261   estimator of the relative mass variation curve slope:

$$\varepsilon(t) = \frac{\left(\frac{\Delta m}{m}\right)(t+1) - \left(\frac{\Delta m}{m}\right)(t)}{\left(\frac{\Delta m}{m}\right)(t)} \qquad (15)$$

263   where $\left(\frac{\Delta m}{m}\right)(t)$ and $\left(\frac{\Delta m}{m}\right)(t+1)$ are the relative mass variations at time t and one day after respectively.

264   From a practical point of view the ε values were estimated using the equation proposed by Baroghel-

265   Bouny [55] to fit the sample mass loss evolution:

$$\left(\frac{\Delta m}{m}\right)(t) = \frac{A\sqrt{t}}{B + \sqrt{t}} \qquad (16)$$

267   where *A* and *B* are two parameters to be fitted on the experimental results. The samples were let to

268   equilibrate in their containers as long as possible but they all met the following requirement: $\varepsilon \leq 0.05\%$

269   (note that many sets of specimens presented lower ε values at the end of the test). A graphical

270   illustration of this requirement significance is presented on Figure 1 for the CEM I specimens kept at 80°C

271   and 76% RH. The criterion was reached after 121 days. Leaving the samples for 121 more days (the

272   equilibration time was then increased by 100%) brought little improvement: the difference between the

273   relative mass variations at 121 and 242 days is about 3.5% (relative value). This value was found to be

274   lower than the variability induced by the use of a different sample-set for each RH. The resulting ε value
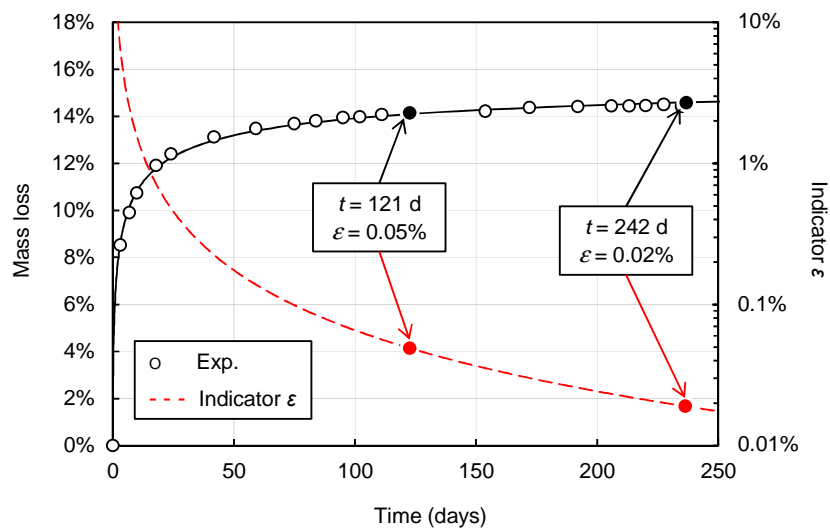
275   was then 0.02%.

276

277   *Figure 1. Illustration of the criterion $\varepsilon \leq 0.05\%$ for the CEM I paste kept at 80°C and 76% RH (in this*

278   *example A=-16.04% and B=1.522 $d^{0.5}$). Note the log-scale for the indicator ε.*

279

280   Once the equilibrium was reached for all the sets of specimens (that is to say when ε was lower than

281   0.05%), the desorption isotherm could be evaluated using the initial properties (specific gravity d_s and

15

282   porosity Ø) and the relative mass variations at equilibrium. It was found convenient to describe the

283   pastes saturation state using the water content *w* which is defined as the ratio of water to dry solid by

284   mass. In our case it could be easily calculated using the following equation:

285    $$w(T,h) = \frac{d_s}{d_s - \emptyset}\left[\frac{\emptyset}{d_s} + \left(\frac{\Delta m}{m}\right)(T,h)\right]$$ (17)

286   where $\left(\frac{\Delta m}{m}\right)(T,h)$ is the relative mass variation at equilibrium with the relative *h* for the temperature *T*.

287   To ensure comparison between the desorption isotherm for the three temperatures a common

288   reference dry state is necessary because temperature affects the free water amount. For instance drying

289   at 20°C using silica gel (RH=3%) as proposed by Baroghel-Bouny [19, 56] is unsuitable here. It is known

290   that heating at 80°C is harmful for cementitious materials mineralogy and microstructure [57-60]. Yet as

291   far as only the first desorption is concerned (no preliminary drying and no further resaturation) drying at

292   80°C (using $CaCl_2$) was chosen here for commodity. In so doing, it was implicitly assumed that the

293   80°C-induced degradation influence on total porosity could be neglected. The authors acknowledge that

294   drying at 80°C is not the common procedure. The reader should remind that porosity was also measured

295   using different protocols (Table 8) and it is possible to use eq. (18) to recalculate the desorption

296   isotherms (for instance 105°C).

297   Two different models were used to fit the desorption isotherms: Mualem-van Genuchten equation (eq.

298   8) was used for unsaturated water transport and Pickett's model was used for adsorption physics. The

299   model proposed by Pickett is considered by the authors to be the only simple model describing the

300   physics of adsorption that can efficiently fit the results (type IV isotherms). Using a model based on

301   adsorption physics instead of that of van Genuchten also proved to ensure a better estimation of the

302   water content at 20% and isosteric energy q_{st}. Pickett's equation is an evolution of the well-known BET

303   model. It can be written under the following form:

$$w = C^P w_m^P \frac{(1-h^n)h + bnh^n(1-h)}{(1-h)[(1-h) + C^P(h + bh^n)]} \tag{18}$$

304

305   where:

306   • C^P is a positive constant that is related to the energy of adsorption of the first layer;

307   • w_m^P the monolayer value corresponds to the water content that is needed to complete a

308   monomolecular layer;

309   • n represents the maximal number of adsorbed layers;

310   • b is related to the rate of evaporation/condensation of water molecules in the layers.

311   ### 3.5. Permeability assessment

312   We did not measure directly the intrinsic permeability K (m^2), for instance using water permeametry [61]

313   because such results are known to be unsuitable for the simulation of unsaturated water flow in

314   concretes [22]. The intrinsic permeability was rather evaluated through inverse analysis as already

315   proposed [20, 21]. For this purpose, the biggest cylinders (Ø51×H60 mm) were put in climatic chambers

316   using the constant environmental conditions reported in Table 5. Periodically the chambers were opened

317   and the samples weighed. The tests were conducted for 65 days for 20°C and 14 days for 50 and 80°C

318   respectively.

319

320   *Table 5. Tests conditions for intrinsic permeability assessment tests.*

Temperature	20°C	50°C	80°C	Unit
RH	54%	85%	85%	-
Liquid pressure (eq. 4)	-83.29	-23.96	-25.78	MPa
Duration	65	14	14	days

321

322 The experimental mass variations were then described using the simplified approach detailed in part 2.

323 From a practical point of view, the finite-element code Cast3m[1] was used to solve eq. (7) and compute

324 the resulting theoretical mass variation. Different intrinsic permeability values were used and the best

325 value was selected using a least-squares minimization process. For more detail about the fitting process

326 the reader is referred to [23]. A quarter of the specimen was described in axisymmetric conditions

327 (Figure 2). 7200 four-node quadrangles (80×90) were used. The time steps were adjusted to ensure

328 convergence (from a few seconds at the beginning of the simulations to one day at the end).

329

330
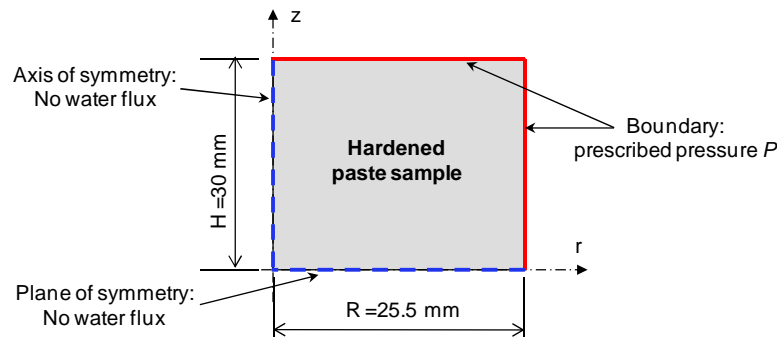
331   *Figure 2. Schematic description of the numerical simulations for permeability assessment.*

332

333 The heating stage was not described (the temperature was assumed to be constant). The initial

334 conditions were: uniform temperature (20, 50 or 80°C) and liquid pressure P=0.0 MPa (saturation). At

335 t=0, a constant pressure (Dirichlet condition) was prescribed all over the sample boundary (the

336 corresponding values are listed in Table 5).

---

[1] http://www.cast3m.org

4. Results

4.1. Feedback on the use of saturated salt solutions

Two major drawbacks were encountered when using saturated salt solutions. First, we did not find this method to be successful for RH regulation: a good illustration is given on Figure 3. We prepared a sodium carbonate (Na_2CO_3) solution in a four-liter desiccator (the same kind as the ones used for the water retention curve characterization) and left it four days in an oven at 80 ± 1°C. Temperature and RH were constantly recorded using a commercial hygrometer: the RH target (85%, Table 4) was quickly reached. After four days, we opened the desiccator and introduced four (saturated) paste specimens. The RH within the desiccator then quickly increased to reach saturation (100%) due to the water release by the four specimens. The RH only began to decrease 11 days after the samples introduction and returned to the target value 14 days after.
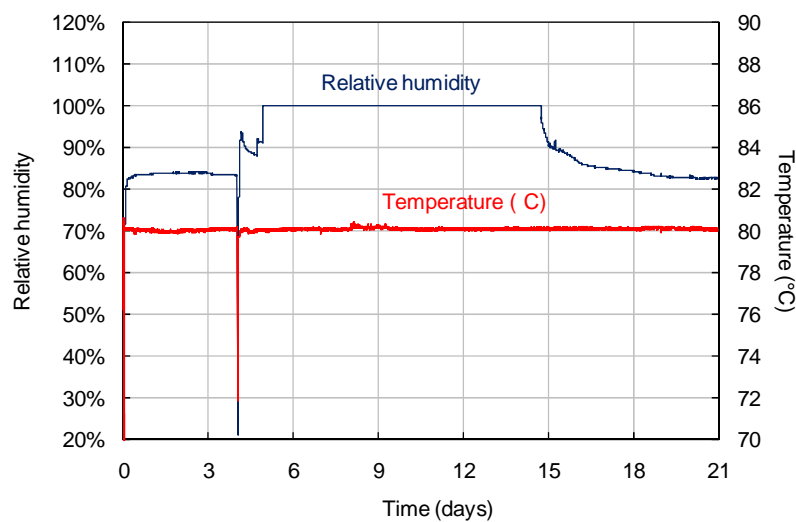

Figure 3. RH and temperature evolution within a desiccator after the insertion of four paste samples (the salt used is Na_2CO_3 resulting in RH=85% at 80°C).

352

353   In this example, only four specimens were introduced whereas sixteen of them were used in the water

354   retention curve experiments. In so doing, we did not expect the salt solutions to successfully maintain

355   the RH in the short term for the three tested temperatures. We believe that it did result in increasing the

356   time needed to reach equilibrium: the resulting mass loss evolutions of the specimens could not be used

357   for water transport properties evaluation. This explains why supplementary isothermal drying tests were

358   conducted for permeability assessment. In a more general way, when using saturated salt solutions to

359   maintain constant conditions one should at least monitor the RH evolution or if possible adjust the

360   chamber volume to the specimens water release rate and salt used.

361   The second major problem we had to face was the crystallization of salt above the solution on the

362   desiccator walls which could eventually come in contact with the specimens and result in unacceptable

363   pollution. This was believed (but it was not verified) to be due to the handling operations needed to have

364   the samples weighed (periodical withdrawal from the oven which could project some solution on the

365   desiccator walls) and to the supersaturation induced by the solution cooling and drying (due to the

366   desiccator opening). This was hindered by periodical examination (twice a week) of all the desiccators to

367   check the salt crystallization. When present, the desiccator walls were thoroughly rinsed and dried using

368   pure water and a clean towel. When the time between two remediation operations was too small, both

369   desiccator and salt solution were eventually changed. The salts under discussion are sodium bromide

370   (NaBr) which was found to be difficult to use at 50 and 80°C whereas sodium chloride (NaCl), potassium

371   chloride (KCl) and to a lesser extent magnesium chloride ($MgCl_2$) were only troublemaking at 80°C.

4.2. Mineralogical composition

373   The contents of portlandite and C-S-H of each paste are presented on Table 6. The CEM I and CEM II

374   pastes showed pretty similar results (despite the limestone filler substitution). As expected, the Low-pH

mix was free of portlandite as already observed by Codina et al. [38]. As a consequence of pozzolanic

reactions, the C-S-H content was high (7.4 mol/L). The CEM V paste laid between the CEM I and the Low-

pH pastes (2.1 mol/L).

Table 6. Portlandite and C-S-H contents of the pastes after the cure.

Phase	CEM I	CEM II	CEM V	Low-pH	Unit
Portlandite	5.6	5.4	2.1	0.0	mol/L of paste
C-S-H	5.1	5.0	7.0	7.4	mol/L of paste

A few TGA tests were also conducted using some of the specimens kept at 80°C (and $CaCl_2$) for the

desorption isotherm characterization. The portlandite content of the CEM I paste was found to be almost

constant versus RH whereas that of the CEM V paste decreased when RH was increased. This was taken

as an indication of ongoing hydration (due to pozzolanic reactions) in the case of the blended cements

(CEM V and Low-pH). We believe that this might have had an impact on the resulting water retention

curves (especially at high RH and temperature) but we were unable to quantify it.
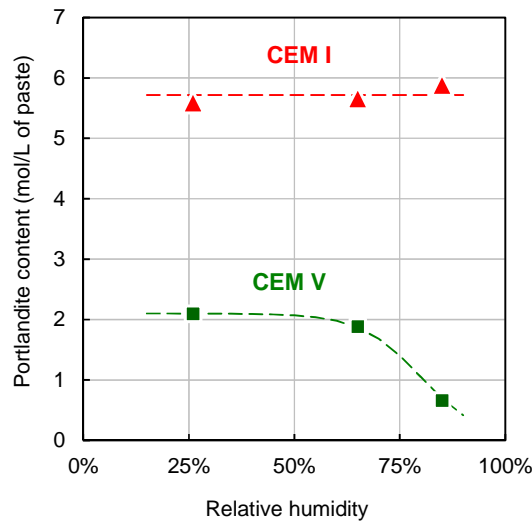

Figure 4. Portlandite content of the CEM I and CEM V pastes kept at 80°C (dashed lines are guides for the

eye only).

389 ### *4.3. Porosity and microstructure*

390 The specific gravity of the saturated pastes d_s was measured using 134 specimens for each paste (Table

391 7). The mean values span from 1.73 (Low-pH) to 2.04 (CEM I): the value decreases when the amount of

392 supplementary cementing materials is increased. Table 8 summarizes the porosity results: the higher the

393 temperature, the higher the porosity. Yet whatever the drying temperature, the porosity value increases

394 with the amount of SCM. Table 9 presents the specific surface area values obtained for each paste using

395 MIP and the desorption isotherms (BET). Here again, the value of the specific surface area increases with

396 the amount of SCM in relation to the increased C-S-H content. The value obtained using the BET model is

397 always significantly higher than that of MIP.

398 *Table 7. Specific gravity of the pastes (standard deviation in brackets).*

Paste	CEM I	CEM II	CEM V	Low-pH
Saturated specific gravity d_{sat}	2.04 (0.01)	1.99 (0.01)	1.93 (0.01)	1.73 (0.01)

399

400 *Table 8. Porosity as a function of drying temperature.*

Temperature	Desiccant	RH	CEM I	CEM II	CEM V	Low-pH
20°C	SiO_2	≈3%	30.4%	31.0%	28.5%	32.1%
50°C	SiO_2	≈3%	35.2%	35.9%	34.2%	40.3%
80°C	$CaCl_2$	≈0%	37.2%	39.5%	38.9%	41.3%
105°C	-	-	38.5%	40.4%	39.1%	45.7%

401

402 *Table 9. Specific surface area of the four pastes.*

Paste	CEM I	CEM II	CEM V	Low-pH	Unit
Specific surface area (BET)	190	199	297	380	m^2/g
Specific surface area (MIP)	30	31	59	113	m^2/g

403

404   The MIP results are presented on Figure 5. The CEM I & CEM II pastes exhibited almost the same pore-

405   size distribution. The CEM V and Low-pH pore-size distributions showed an important reduction of the

406   pores of diameter larger than 50 nm (despite the presence of an unexpected and unexplained pore

407   population around 200 nm for the CEM V) together with an important increase of pores of diameter

408   lower than 50 nm. This was attributed to the presence of SCMs in the CEM V and Low-pH mix leading to

409   supplementary C-S-H formation (see Table 6).

410
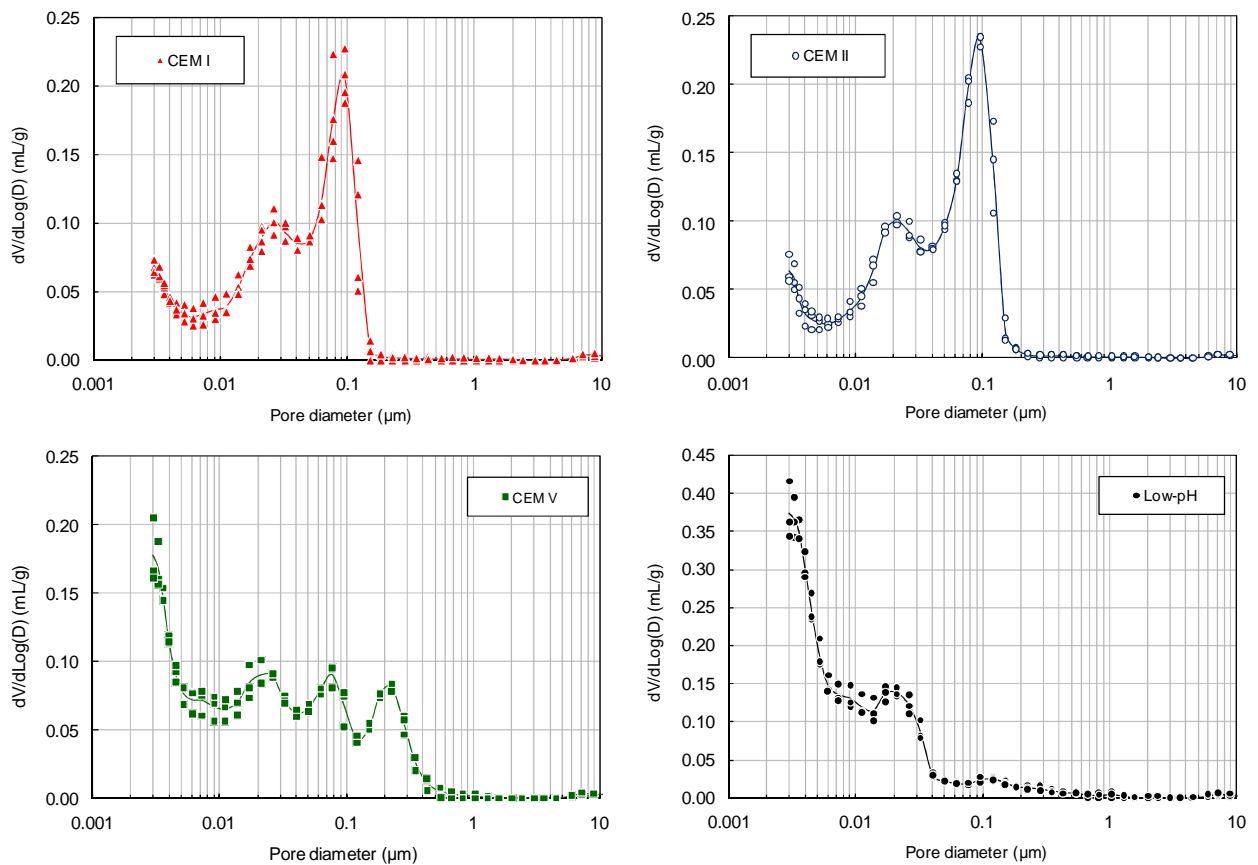
411   *Figure 5. Pore-size distribution of the four hardened cement pastes as obtained using MIP and samples*

412   *dried at 20°C (using silica gel and then freeze-drying).*

413

414   The MIP results obtained using heated specimens are depicted on Figure 6. Whatever the considered

415   paste, heating led to the coarsening of the pore structure: that is to say the increase of both capillary

416   porosity and critical pore radius (corresponding to the sudden slope change in the MIP results). As

417   suggested by Brue et al. [14] ettringite dissolution [62, 63] as well as C-S-H alteration [64-66] can be

418   considered as the major causes of the pore structure modifications.

419
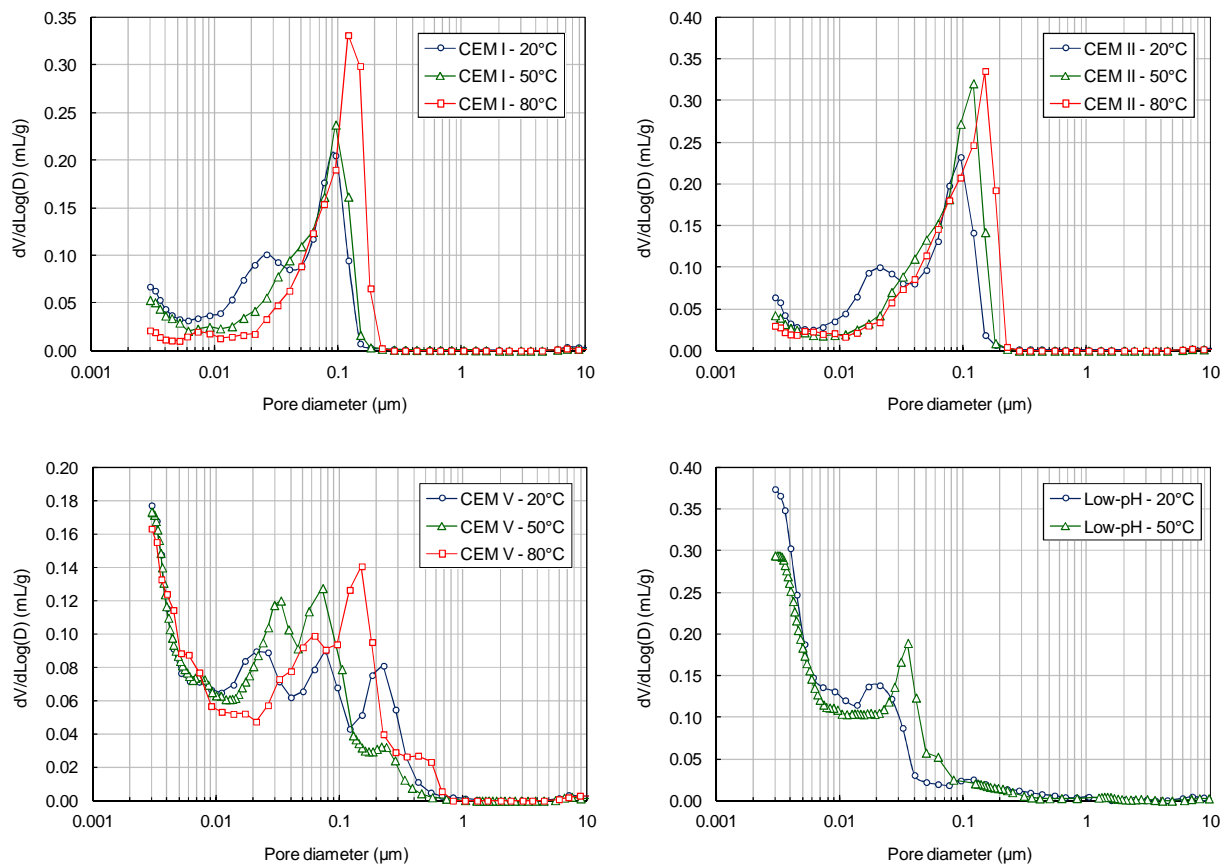
420   *Figure 6. Pore size distribution versus temperature as obtained using MIP. Each curve corresponds to the*

421   *mean result of 3 or 4 tests. It was not possible to obtain reliable and repeatable results for the Low-pH*

422   *samples kept at 80°C: these results are not presented.*

423 **4.4. Desorption isotherms**

424 The first desorption isotherm at 20°C of the four pastes are presented on Figure 7. The depicted curves

425 are of type IV according to the classification originally proposed by Brunauer [46, 67]: one can note the

426 monomolecular layer edification at low RH as well as the presence of a plateau near saturation (at least

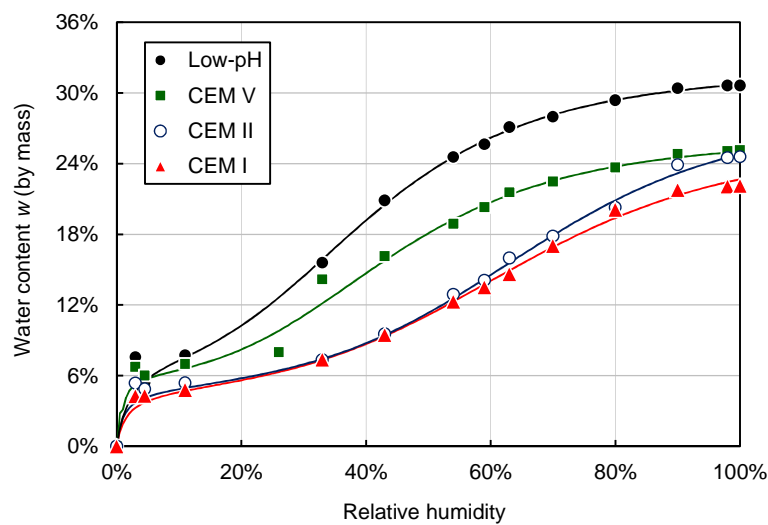427 for CEMV and Low-pH) representative of capillary condensation within a meso-porous medium.

428

429

430 *Figure 7. First desorption isotherm at 20°C for the four pastes. Each symbol corresponds to the mean*

431 *value of each sample set (at least three samples) whereas the solid lines (Pickett's model) are just guides*

432 *for the eye.*

433 Similarly to the MIP results, the CEM I and CEM II pastes exhibit almost the same desorption curve

434 despite the 25% clinker-substitution by carbonate filler. The two curves differ at high RH: the CEM II

435 paste retains more water at saturation than the CEM I due to higher porosity. This isotherm shape is very

436 similar to the ones obtained using ordinary cementitious materials (pastes and concretes, w/c from 0.35

437 to 0.45) by Baroghel-Bouny [56]. The CEM V and Low-pH pastes show a different general pattern. The

438   presence of a plateau near saturation (RH=100%) is much more noticeable than for CEM I & II: the

439   desorption isotherm slope at high RH is lower than the ones of CEM I & II (due to a refined pore size

440   distribution). The water content at low RH (typically for monomolecular adsorption) is also higher than

441   for CEM I & II due to higher C-S-H content.

442   The impact of temperature on the water retention curve is depicted on Figure 8. Whatever the

443   considered paste a temperature increase induces the reduction of the water retained at equilibrium with

444   any arbitrary RH. This effect was observed over the whole RH-range and even at RH=100% for the CEM I

445   and CEM II pastes but was hardly observed for the CEM V and Low-pH pastes. This was attributed to the

446   effect of ongoing hydration as detected using TGA: the resulting mass gain helped reduce the fall in
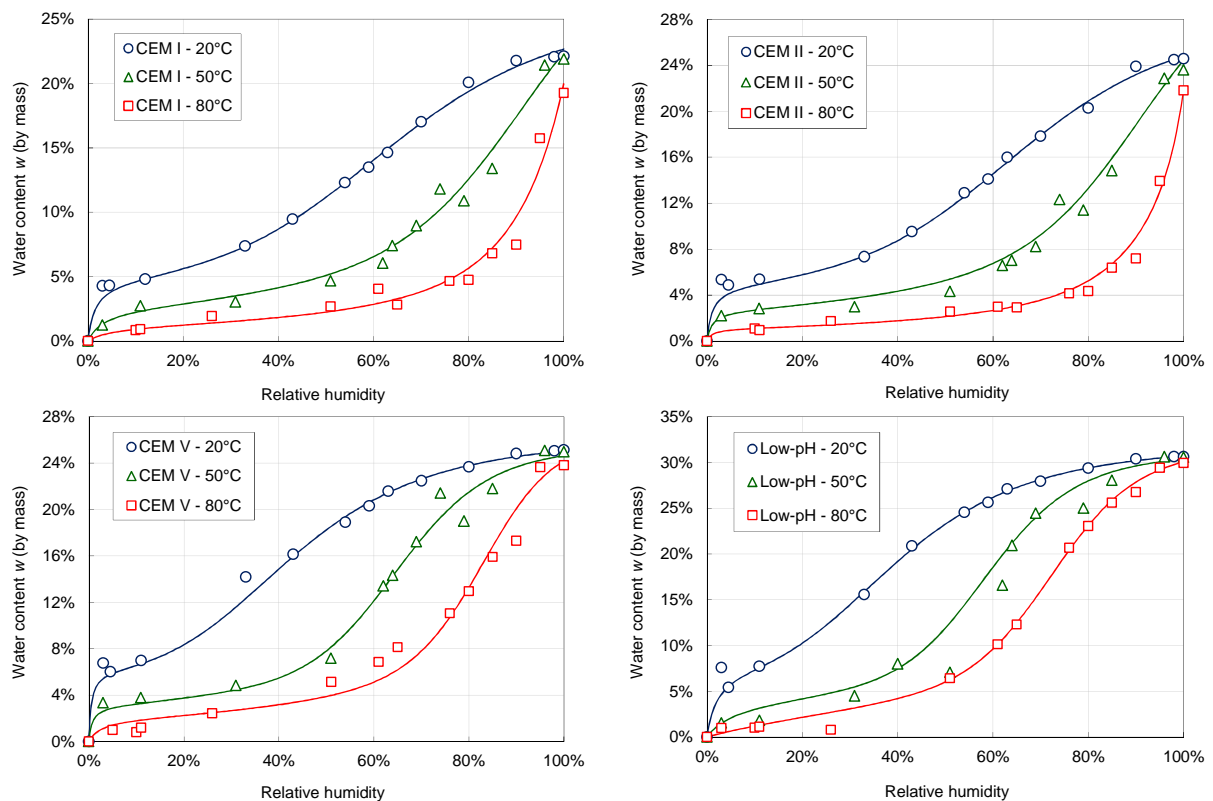
447   water content at high RH.

448   *Figure 8. Desorption isotherm of the four hardened pastes as a function of temperature (water content).*

449   *Each symbol corresponds to the mean value of each sample set (at least three samples) whereas the solid*

450   *lines stand for the interpolation using Pickett's model.*

451   ### *4.5. Isoteric energy*

452   The isoteric energy of adsorption q_{st} was assessed using eq. (1). The RH *h* at equilibrium with the water

453   content *w* was evaluated using Pickett's model (eq. 18) and the vapor pressure p_v was calculated using

454   Rankine's equation:

455    $$p_v(w,T) = h(w,T)p_{vs}(T) = h(w,T)P_a exp\left(\alpha - \frac{\beta}{T}\right) \tag{19}$$

456   with P_a=101325 Pa; α = 13.7 and β = 5120 K. The function used to interpolate $p_{vs}(T)$ is of first

457   importance because it appeared to influence the results obtained (the evolution remains unchanged but

458   the values are modified). The resulting isoteric energy evolutions are plotted on Figure 9 as functions of

459   coverage $\frac{w}{w_m}$ (number of adsorbed layers). This presentation allows the results to be fully comparable

460   (and not to depend on density and porosity). Apart from the Low-pH mix all the curves exhibit the same

461   evolution: q_{st} increases at low coverage (typically between 0.0 and 0.5) from 70 kJ/mol to reach a

462   maximal value (around 100 kJ/mol) and then continuously decreases to get close to the average water

463   enthalpy of condensation (43.7 kJ/mol between 20 and 80°C) at high coverage. Note that the uncertainty

464   related to the maximal isoteric evaluation process was estimated to ± 10 kJ/mol.
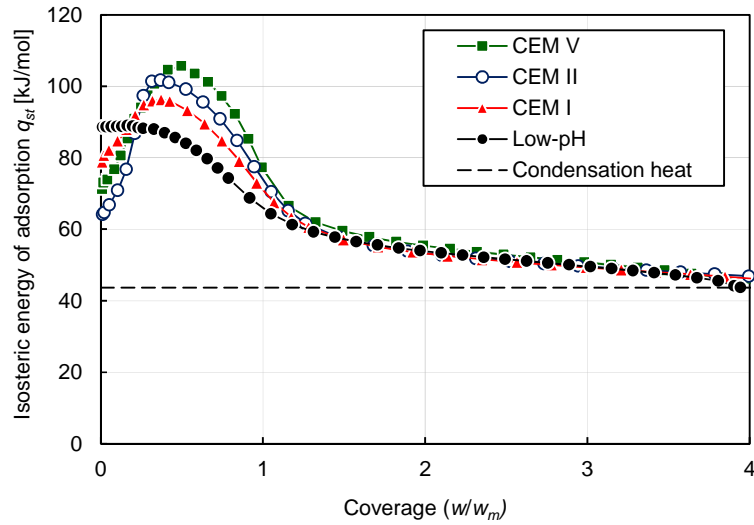
465

Figure 9. Isosteric energy of adsorption q_st of the four considered hardened cement pastes.

Most of q_{st} variations can be observed in the first layer (that is to say for w/w_m less than 1.0) which is representative of the strong interaction between the first water layer and the hardened cement paste. The q_{st} decrease (for w/w_m greater than 0.5) is representative of the decrease of the cementitious material influence with the increase of the distance between the newly adsorbed water molecules and substrate. The asymptotic value for high coverage (43.7 kJ/mol) corresponds to the average water condensation energy (between 20 and 80°C): it can be considered that there is no more influence of the cementitious material substrate and all water molecules are bonded the ones to the others (liquid state representative of capillary condensation).

An increase in q_{st} in the first layer is not common: monotonic decrease is generally observed. In our case, the maximum might just be due to the isosteric energy estimation process (use of Pickett's model rather than another arbitrary function for instance) and to the lack (and variability) of the experimental results in the monolayer zone (between 0 and 30% RH). Yet a maximum has already been observed for different

481 materials [68-76]. For hydrophobic materials such as activated carbons [70, 71] q_{st} increases from low

482 values at low coverage (due to the lack of hydrophilic sites) up to the condensation enthalpy in relation

483 to the formation of water clusters. For hydrophilic materials the increase is usually explained by the

484 swelling of the dry matrix resulting in the exposure of new adsorption sites of high binding energy. When

485 all the high energy sites are occupied water adsorption occurs on less energetic sites leading to the q_{st}

486 decrease. In the case of cementitious materials, the q_{st} increase might be due to the desaturation and

487 the subsequent collapse of the C-S-H interlayer space [77, 78] preventing water access to high-binding

488 energy adsorption sites within the C-S-H interlayer. This simple assumption would deserve additional

489 experiments to be confirmed (or infirmed).

490 Figure 10 presents the comparison between the isosteric energy obtained in this study (open circles) for

491 the CEM I paste and the corresponding concrete (filled circles) [13, 17]. It is obvious that the two

492 evolutions do not match: the maximal value obtained for the concrete is about 66 kJ/mol whereas it

493 reaches 100 kJ/mol for the paste. One could then conclude that there is no consistency between these

494 two results. As a matter of fact, two different models were used to describe the desorption isotherm in

495 both cases: GAB and Pickett models for the concrete and the paste respectively. These models were used

496 to calculate the RH (and then the vapor pressure) at equilibrium with any arbitrary water content as

497 needed for Clausius-Clapeyron equation, see [17] for more details. When we used Pickett's model to

498 evaluate the concrete isosteric energy from the CEM I paste results we obtained an almost perfect

499 match. The equation used for the description of the water retention curve (GAB or Pickett in our case)

500 appears to be very important since it greatly influences the resulting isosteric energy q_{st}. As a

501 consequence when handling such data, one has to be very careful and be consistent in the choice of the

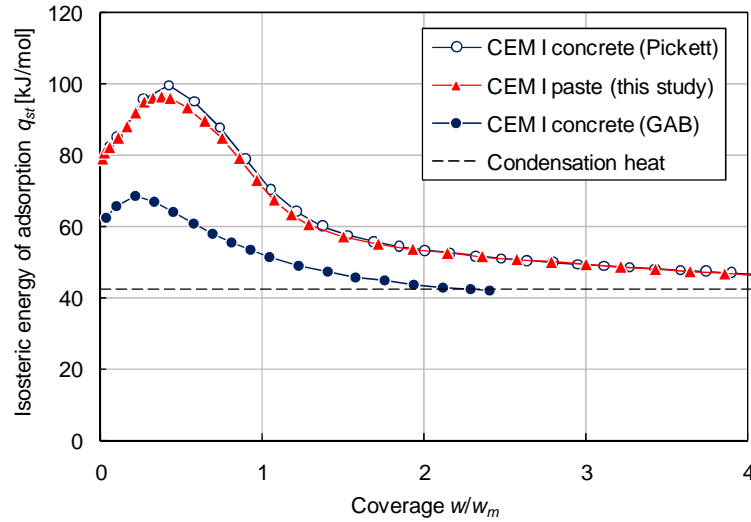502 model used to describe the water retention curve in order to avoid erroneous results.

503

504   *Figure 10. Comparison between the isosteric energy evolutions obtained in this study and in a previous*

505   *study [13, 17].*

506

507   This good isosteric energy correspondence was also supported by the comparison between paste and

508   concrete desorption isotherm as shown in Figure 11. Figure 11 (a) presents the experimental desorption

509   isotherm at 80°C for the CEM I paste tested in this study and the corresponding concrete studied in [13].

510   To make the two isotherms comparable (porosity and density are different) the water content w was

511   divided by its maximal value w_{max}. The two datasets describe almost the same curve (despite the

512   variability). Figure 11 (b) presents the comparison between the CEM I concrete desorption isotherm

513   acquired at 30°C and the CEM I paste curve estimated using Clausius-Clapeyron and Pickett's model and

514   the corresponding isosteric energy q_{st} (Figure 10). Once again, the comparison is very good. It is known

515   that for high-performance materials the presence of aggregates does not influence the water retention

516   curve [55, 56]: these results also show that it does not influence the isosteric energy (that is to say the

517   variation induced by temperature).

518
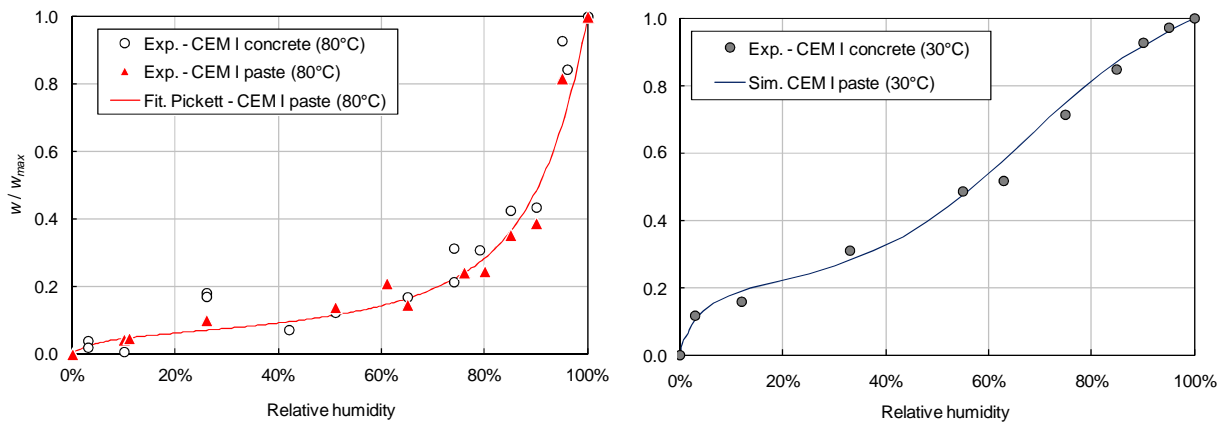
(a) Desorption isotherms at 80°C (CEM I paste and

corresponding concrete)

(b) Desorption isotherm at 30°C

519   *Figure 11. Comparison between the desorption isotherms of the CEM I paste tested in this study and the*

520   *corresponding concrete [13].*

521   **4.6. Water transport**

522   Figure 12 presents the experimental mass loss evolution of the samples dried at 20°C and 54% RH (the

523   initial mass of the saturated specimens was taken as reference/standard to compute mass loss). The

524   CEM II paste exhibited the fastest mass loss (7% after 60 days) far above the CEM I (4.5% after 60 days).

525   Here the effect of the 25% clinker substitution by limestone filler appeared to have a significant impact

526   (unlike the pore-network distribution and desorption isotherm). The CEM V and Low-pH pastes showed

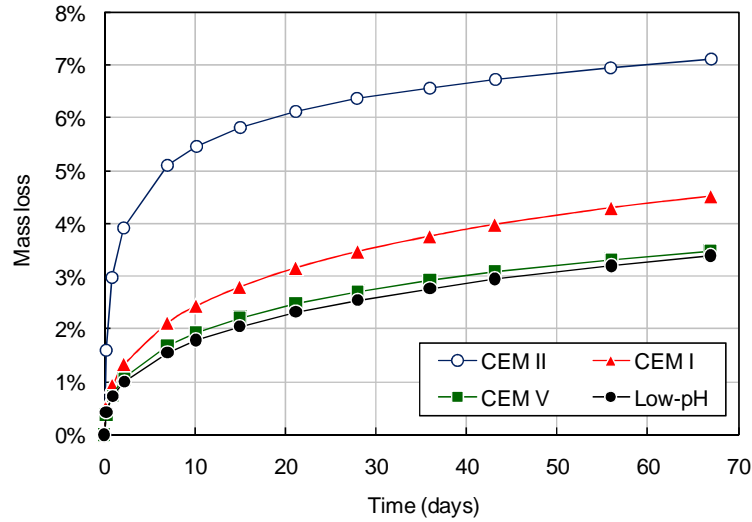527   almost the same mass loss evolution (3.3% after 60 days).

Figure 12. Experimental mass loss of the paste samples dried at 20°C and 54% RH.

The two van Genuchten's parameters P_0 and m needed in eq. (8) were fitted on the experimental

desorption isotherms (Figure 13): the corresponding values are reported in Table 10. At 20°C the values

obtained are consistent with the literature [19, 22, 28]. It is noteworthy that when temperature

increases the m values remain stable whereas those of P_0 decrease. The relative permeability evolutions

at 20°C are depicted on Figure 14 (a). As expected the finer the pore size distribution, the lower the

relative permeability decrease with saturation. The relative permeability evolutions can be classified in

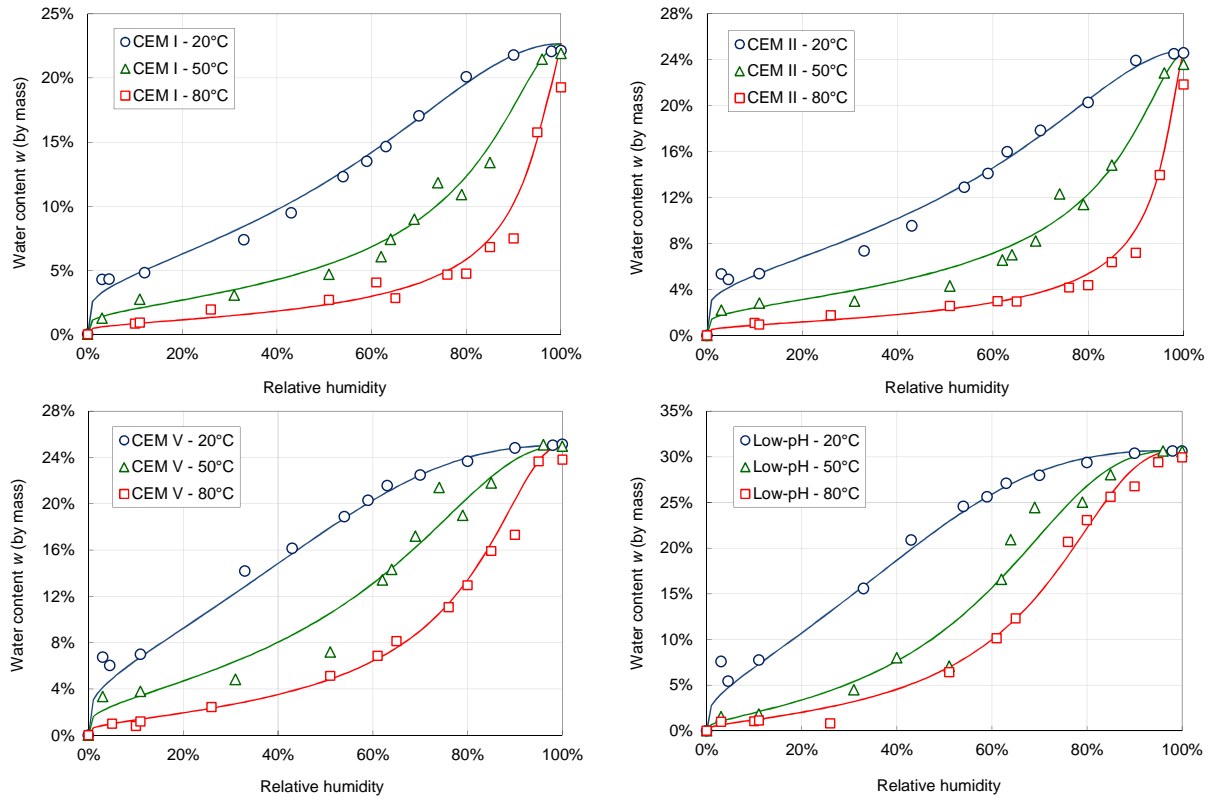the following order: Low-pH > CEM V > CEM I > CEM II.

Figure 13. Desorption isotherm of the four hardened pastes as a function of temperature (saturation) fitted using van Genuchten equation.

Table 10. Van Genuchten parameters and permeability values.

Paste		CEM I	CEM II	CEM V	Low-pH	Unit
20°C	P_0	51.4	42.5	96.9	108.7	MPa
	m	0.465	0.437	0.529	0.578	-
	K	2.0×10^{-22}	8.0×10^{-22}	7.0×10^{-23}	2.5×10^{-23}	m^2
50°C	P_0	18.9	14.7	47.1	56.8	MPa
	m	0.457	0.425	0.506	0.605	-
	K	3.0×10^{-22}	22.0×10^{-22}	3.0×10^{-23}	4.6×10^{-23}	m^2
80°C	P_0	8.1	5.2	23.5	40.3	MPa
	m	0.458	0.436	0.517	0.595	-
	K	140.0×10^{-22}	600.0×10^{-22}	150.0×10^{-23}	18.0×10^{-23}	m^2
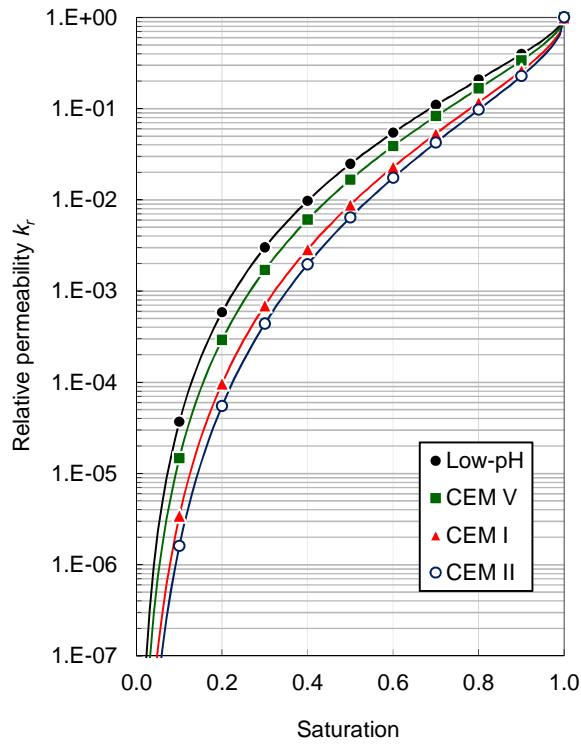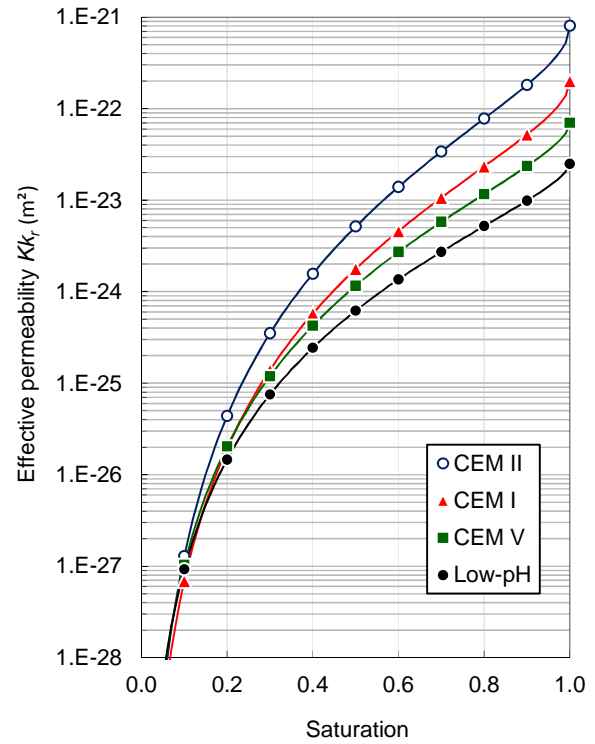
(a) Relative permeability k_r (b) Effective permeability Kk_r

543   *Figure 14. Relative (a) and effective (b) permeability of the four hardened cement pastes at 20°C.*

544   Table 10 recapitulates the intrinsic permeability values assessed using inverse analysis. At 20°C they can

545   be classified in the exact inverse order obtained for the relative permeability as shown in Figure 14 (b):

546   CEM II > CEM I > CEM V > Low-pH. This order is consistent with the pastes pore-network fineness as well

547   as the C-S-H content. Figure 15 presents the permeability variations induced by temperature. Unlike the

548   results of Powers [5], they could not be described the classical Arrhenius law (the points were not

549   aligned in the log-scale plot). For fitting purposes a double exponential law (eq. 20) was alternatively

550   proposed:

551                  $$K(T) = K_0 exp\left[exp\left(\frac{T-293.15}{T_c}\right) - 1\right]$$ (20)

552   where K_0 and T_c are two positive parameters, the values of which are reported in Table 11. It has to be

553   noted that the CEM V paste showed an unexpected and unexplained permeability decrease between 20

554   and 50 °C which cannot be described using eq. (18).

555
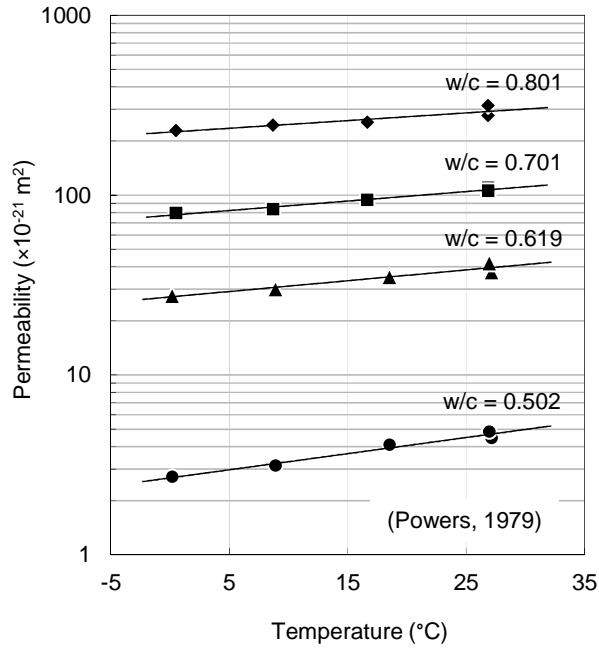
(a) Direct measurement from Powers (1979)   (b) Inverse analysis from this study
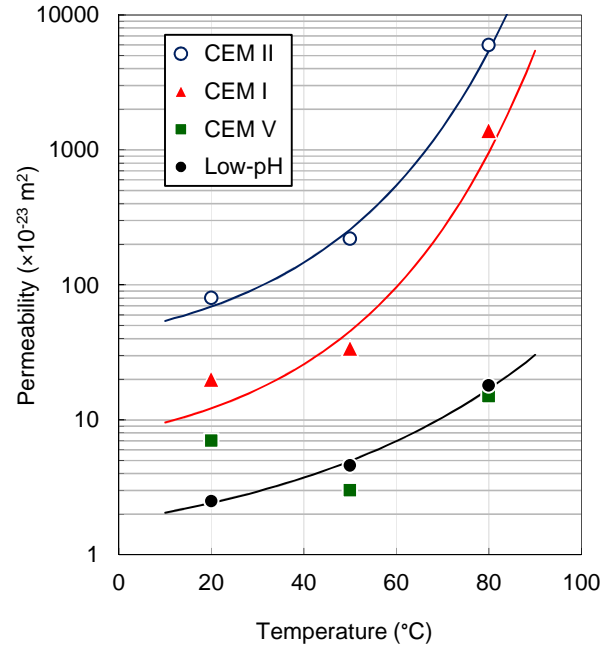
556   *Figure 15. Permeability versus temperature: (a) following Powers [5], using water permeametry between*

557   *0 and 30°C and (b) inverse analysis from this study.*

558   *Table 11. Parameters for the description of temperature influence on permeability (eq. 20).*

Parameter	CEM I	CEM II	CEM V	Low-pH	Unit
K_0	12.2×10^{-23}	69.1×10^{-23}	N/A	2.4×10^{-23}	m²
T_c	35.7	35.7	N/A	55.6	K

5. Discussion

The use of Clausius-Clapeyron to describe the water retention curve temperature induced modifications implicitly assumes that the cementitious material pore structure remains unchanged. This assumption was found to be acceptable for a high-performance concrete between 30 and 80°C [13]. The coarsening of the pore structure observed using MIP in this study (from 20 to 80°C) is supported by the permeability results and the unsuccessful comparison with the results of Powers [5] (Figure 15). He showed that between 0 and 30°C (temperature range within which no temperature induced modification of the pore structure was expected) the permeability variations can be fitted by a classical Arrhenius law. In our case the permeability variations are too big to be fitted by such a function. This is consistent with an increase of the transport properties associated to porosity opening. There is however other potential causes of the important permeability increase. Heating up to 80°C might have caused microcracking or increased the contribution of water transport in the gaseous phase which is not accounted for in our simplified approach. This might have resulted in overestimating the pastes permeability values at high temperature.

The coarsening of the pore structure observed calls into question the use of Clausius-Clapeyron and the corresponding assumption of unaltered microstructure. Indeed it is true that the pore structure coarsens when temperature increases: the error induced by our assumption also increases with temperature. Nevertheless, we believe that thermal desorption is the major mechanism at work for moderate temperatures (let us state up to 50°C). For temperatures up to 80°C, alteration of the pore structure might have a non-negligible impact on the water retention curve. Unfortunately there is nowadays no way to quantify the link the pore structure determined using MIP and the water retention curve and Clausius-Clapeyron remains the only available tool to describe the influence of temperature. Consequently it is difficult to estimate the error associated to our assumption. In a simple way one could

582 characterize the water retention curves at 20°C of samples preliminary treated at higher temperatures

583 (from 20 to 80°C) and analyze the results to evaluate the contribution of the microstructure variation.

6. Conclusion

585 Temperature has a great importance for water transport in cementitious materials. This issue is of first

586 importance for the durability assessment of reinforced concrete structures for radioactive waste

587 management. An experimental campaign was then designed to determine the influence of temperature

588 on cementitious materials water transport properties. Four hardened cement pastes of interest for

589 radioactive waste management were selected. Using a simplified approach, the transport of water was

590 described using liquid permeation only. This allowed reducing the number of properties to acquire

591 experimentally: porosity, water retention curve and (intrinsic and relative) permeability.

592 The water retention curve was characterized using the saturated salt solution method. The unsaturated

593 permeability was assessed using inverse analysis making use of the Mualem-van Genuchten model.

594 Three temperatures were tested: 20, 50 and 80°C. As expected, temperature was found to have a great

595 impact on the water retention curve: a temperature increase decreased the water content at equilibrium

596 for all the pastes. The intrinsic permeability value significantly increased with temperature, but the data

597 obtained do not follow Arrhenius activation law. These results constitute a valuable and consistent data

598 set for the description of water transport in the field of radioactive waste management.

599 The temperature induced alteration of the water retention curves were described using Clausius-

600 Clapeyron equation and the corresponding isosteric energy of adsorption was evaluated. In so doing, the

601 microstructure was assumed not to be altered during the heating. The coarsening of the pore structure

602 subsequent to heating was however highlighted using MIP. The water retention curve modifications

603 were then assumed to result from a combination of thermal desorption (described by Clausius-Clapeyron

604 equation) and pore structure coarsening. The influence of the latter remains to be evaluated.

605 **Acknowledgements**

7. References

608 [1] K. Tuutti, Corrosion of steel in concrete, Swedish Cement and Concrete Research Institute, 1982, pp.

609 468.

610 [2] B.P. Hughes, I.R.G. Lowe, J. Walker, The diffusion of water in concrete at temperatures between 50

611 and 95°C, British Journal of Applied Physics, 17 (1966) 1545-1452.

612 [3] N.L. Hancox, The role of moisture diffusion in the drying of cement paste under the influence of

613 temperature gradients, Journal of Physics D: Applied Physics, 1 (1968) 1769-1777.

614 [4] G.M. Glover, E. Rassk, Water diffusion and microstructure of hardened cement pastes, Materials and

615 Structures, 5 (1972) 315-322.

616 [5] T.C. Powers, The specific surface area of hydrated cement obtained from permeability data, Materials

617 and Structures, 12 (1979) 159-168.

618 [6] J.-F. Daïan, Condensation and isothermal water transfer in cement mortar, part I - pore size

619 distribution, equilibrium, water condensation and imbibition, Transport in Porous Media, 3 (1988) 563-

620 589.

621 [7] S.F. Wong, T.H. Wee, S. Swaddiwudhipong, S.L. Lee, Study of water movement in concrete, Magazine

622 of Concrete Research, 53 (2001) 205-220.

623 [8] R. Černy, J. Drchalová, P. Rovnaníková, The effects of thermal load and frost cycles on the water

624 transport in two high-performance concretes, Cement and Concrete Research, 31 (2001) 1129-1140.

625   [9] M. Jooss, H.W. Reinhardt, Permeability and diffusivity of concrete as function of temperature,

626   Cement and Concrete Research, 32 (2002) 1497-1504.

627   [10] J. Hundt, H. Kantelberg, Sorptionsuntersuchungen an zemestein, zementmörtel und beton (in

628   german), Deutscher Ausschuss für Stahlbeton, Heft 297 (1978) 25-39.

629   [11] F. Radjy, E.J. Sellevold, K.K. Hansen, Isosteric vapor pressure-temperature data for water sorption in

630   hardened cement paste: enthalpy, entropy and sorption isotherms at different temperatures, Report

631   BYG-DTU R057, Technical University of Denmark (DTU), Lyngby, Denmark, 2003, pp. 58.

632   [12] T. Ishida, K. Maekawa, T. Kishi, Enhanced modeling of moisture equilibrium and transport in

633   cementitious materials under arbitrary temperature and relative humidity history, Cement and Concrete

634   Research, 37 (2007) 565-578.

635   [13] S. Poyet, Experimental investigation of the effect of temperature on the first desorption isotherm of

636   concrete, Cement and Concrete Research, 39 (2009) 1052-1059.

637   [14] F. Brue, C.A. Davy, F. Skoczylas, N. Burlion, Effect of temperature on the water retntion properties of

638   two high-performance concretes, Cement and Concrete Research, 42 (2012) 384-396.

639   [15] J. Jiang, Y. Yuan, Relationship of moisture content with temperature and relative humidity in

640   concrete, Magazine of Concrete Research, 65 (2013) 685-692.

641   [16] M. Wu, B. Johannesson, M. Geiker, A study of the water vapor sorption isotherms of hardened

642   cement pastes: possible pore structure changes at low relative humidity and the impact of temperature

643   on isotherms, Cement and Concrete Research, 56 (2014) 97-105.

644   [17] S. Poyet, S. Charles, Temperature dependence of the sorption isotherms of cement-based materials:

645   heat of sorption and Clausius-Clapeyron formula, Cement and Concrete Research, 39 (2009) 1060-1067.

646   [18] H. Pan, J.A. Ritter, P. Balbuena, Examination of the approximations used in determining the isosteric

647   heat of adsorption from the Clausius-Clapeyron equation, Langmuir, 14 (1998) 6323-6327.

648   [19] V. Baroghel-Bouny, M. Mainguy, T. Lassabatere, O. Coussy, Characterization and identification of

649   equilibrium and transfer moisture properties for ordinary and high-performance cementitious materials,

650   Cement and Concrete Research, 29 (1999) 1225-1238.

651   [20] M. Mainguy, O. Coussy, V. Baroghel-Bouny, Role of air pressure in drying of weakly permeable

652   materials, Journal of Engineering Mechanics (ASCE), 127 (2001) 582-592.

653   [21] O. Coussy, Poromechanics, John Wiley & Sons Ltd2004.

654   [22] V. Baroghel-Bouny, Water vapour sorption experiments on hardened cementitious materials. Part II.

655   Essential tool for assessment of transport properties and for durability prediction, Cement and Concrete

656   Research, 37 (2007) 438-454.

657   [23] S. Poyet, Determination of the intrinsic permeability to water of cementitious materials: influence of

658   the water retention curve, Cement and Concrete Composites, 35 (2013) 127-135.

659   [24] S. Whitaker, Simultaneous heat, mass, and momentum transfer in porous media: a theory of drying,

660   Advances in Heat Transfer, 13 (1977) 119-203.

661   [25] D. Gawin, B.A. Schrefler, Thermo-hydro-mechanical analysis of partially saturated porous materials,

662   Engineering Computations, 13 (1996) 113-143.

663   [26] J. Selih, A.C.M. Sousa, T.W. Bremner, Moisture transport in initially fully saturated concrete during

664   drying, Transport in Porous Media, 24 (1996) 81-106.

665   [27] F. Meftah, S. Dal Pont, Staggered finite volume modeling of transport phenomena in porous

666   materials with convective boundary conditions, Transport in Porous Media, 82 (2010) 275-298.

667   [28] M. Thiery, V. Baroghel-Bouny, N. Bourneton, G. Villain, C. Stéfani, Modélisation du séchage des

668   bétons, analyse des différents modes de transfert hydrique (in French), European Journal of

669   Environmental and Civil Engineering, 11 (2007) 541-577.

670   [29] M. Thiery, P. Belin, V. Baroghel-Bouny, M.D. Nguyen, Modeling of isothermal drying process in

671   cementitious materials, analysis of the moisture transfer and proposal of simplified approaches, in: J.-F.

672   Shao, N. Burlion (Eds.) 3rd international conference GeoProc, Wiley, Lille (France), 2008, pp. 571-579.

673   [30] L.A. Richards, Capillary conduction of liquids through porous mediums, Physics, 1 (1931) 318-333.

674   [31] B.M. Savage, D.J. Janssen, Soil physics principles validated for use in predicting unsaturated moisture

675   movement in Portland cement concrete, ACI Materials Journal, 94 (1997) 63-70.

676   [32] M.T. van Genuchten, A closed-form equation for predicting the hydraulic conductivity of

677   unsaturated soils, Soil Science Society of America Journal, 44 (1980) 892-898.

678   [33] Y. Mualem, A new model for predicting the hydraulic conductivity of unsaturated porous media,

679   Water Resources Research, 12 (1976) 513-522.

680   [34] H. Lagrave, G. Ranc, C. Gallé, S. Durand, Durability design of heated concrete structures.

681   Methodology and application to long-term interim storage, Journal de Physique IV, 136 (2006) 223-231.

682   [35] J.-P. Silvy, N. Moulin, F. Laurent, Long-term (100-300 years) interim dry storage for spent fuel:

683   package and facilities development including safety aspects and durability assessment program, in: J.D.B.

684   Lambert, K.K. Kadyrzhanov (Eds.) Safety Related Issues of Spent Nuclear Fuel Storage, Springer, 2007, pp.

685   181-188.

686   [36] P. de Coninck, G. Ranc, J. Iacono, J.-L. Martin, N. Moulin, K. Shirai, Y. Le Pape, E. Tronche,

687   Contribution of Galatée on reinforced concretesStructurebBehavior for a full scales subsurface storage

688   laboratory, in: F. Bart, C.C.D. Coumes, F. Frizon, S. Lorent (Eds.) Proceedings of the 1st NUWCEM

689   SymposiumAvignon (France), 2011.

690   [37] C. Cau Dit Coumes, S. Courtois, D. Nectoux, S. Leclercq, X. Bourbon, Formulating a low-alkalinity,

691   high-resistance and low-heat concrete for radioactive waste repositories, Cement and Concrete

692   Research, 36 (2006) 2152-2163.

693   [38] M. Codina, C. Cau-dit-Coumes, P. Le Bescop, J. Verdier, J.P. Ollivier, Design and characterization of

694   low-heat and low-alkalinity cements, Cement and Concrete Research, 38 (2008) 437-448.

695   [39] R. Barneyback, S. Diamond, Expression and analysis of pore fluid from hardened psates and mortars,

696   Cement and Concrete Research, 11 (1981) 279-285.

697   [40] J. Khatib, P.S. Mangat, Absorption characteristics of concrete as a function of location relative to

698   casting position, Cement and Concrete Research, 25 (1995) 999-1010.

699   [41] J. Khatib, P.S. Mangat, Porosity of cement paste cured at 45°C as a function of location relative to

700   casting position, Cement and Concrete Research, 25 (2003) 97-108.

701   [42] E.E. Demirci, R. Şahin, Comparison of carbonation resistance and uniformity of SCC and CC core

702   samples, Magazine of Concrete Research, 2014, pp. 531-539.

703   [43] R.A. Olson, H.M. Jennings, Estimation of C-S-H content in a blended cement paste using water

704   adsorption, Cement and Concrete Research, 31 (2001) 351-356.

705   [44] G. Pickett, Modification of the Brunauer-Emmett-Teller theory of multimolecular adsorption, Journal

706   of the American Chemical Society, 67 (1945) 1958-1962.

707   [45] S. Brunauer, P.H. Emmett, E. Teller, Adsorption of gases in multimolecular layers, Journal of the

708   American Chemical Society, 60 (1938) 309-319.

709   [46] J.B. Condon, Surface area and porosity determinations by physisorption - Measurements & theory,

710   Elsevier2006.

711   [47] P.H. Emmett, S. Brunauer, The Use of Low Temperature van der Waals Adsorption Isotherms in

712   Determining the Surface Area of Iron Synthetic Ammonia Catalysts, Journal of the American Chemical

713   Society, 59 (1937) 1553-1564.

714   [48] S.J. Gregg, K.S.W. Sing, Adsorption, surface area and porosity, 2nd ed ed., Academic Press, London,

715   United Kingdom, 1982.

716 [49] L. Wadsö, K. Svennberg, A. Dueck, An experimentally simple method for measuring sorption

717 isotherms, Drying Technology, 22 (2004) 2427-2440.

718 [50] D.S. Carr, B.L. Harris, Solutions for maintaining constant relative humidity, Industrial and Engineering

719 Chemistry, 41 (1949) 2014-2015.

720 [51] A. Wexler, S. Hasegawa, Relative humidity-temperature relationships of some saturated salt

721 solutions in temperature range 0°C to 50°C, Journal of Research of the National Bureau of Standards, 53

722 (1954) 19-26.

723 [52] A. Scheider, Neue dagramme zur bestimmug der relativen luftfeuchtigkeit uber gesattigten

724 wasserigen salzslosungen und wasserigen schwefelsaurelosingen bei verschiedenen temperaturen (in

725 german), Hol als Rohund Werstoff, 18 (1960) 269-272.

726 [53] J.F. Young, Humidity control in the laboratory using salt solutions - a review, Journal of Applied

727 Chemistry, 17 (1967) 241-245.

728 [54] L. Greenspan, Humidity fixed points of binary saturated aqueous solutions, Journal of Research of

729 the National Bureau of Standards - A, Physics and Chemistry, 81A (1977) 89-96.

730 [55] V. Baroghel-Bouny, Caractérisation des pâtes de ciment et des bétons : Méthodes, analyse,

731 interprétations (in french), Presses du Laboratoire Central des Ponts et Chaussées, Paris, France, 1994.

732 [56] V. Baroghel-Bouny, Water vapour sorption experiments on hardened cementitious materials: Part I.

733 Essential tool for analysis of hygral behaviour and its relation to pore structure, Cement and Concrete

734 Research, 37 (2007) 414-437.

735 [57] C. Gallé, Effect of drying on cement-based materials pore structure as identified by mercury

736 intrusion porosimetry. A comparative study between oven-, vacuum-, and freeze-drying, Cement and

737 Concrete Research, 31 (2001) 1467-1477.

738 [58] M.C. Garci Juenger, H.M. Jennings, The use of nitrogen adsorption to assess the microstructure of

739 cement paste, Cement and Concrete Research, 31 (2001) 883-892.

740 [59] J.J. Beaudouin, B.T. Tamtsia, Effect of drying methods on microstructural changes in hardened

741 cement paste: an A.C. impedance spectroscopy evaluation, Journal of Advanced Concrete Technology, 2

742 (2004) 113-120.

743 [60] A. Korpa, R. Trettin, The influence of different drying methods on cement paste microstructures as

744 reflected by gas adsorption: comparison between freeze-drying, D-drying, P-drying and oven-drying,

745 Cement and Concrete Research, 36 (2006) 634-649.

746 [61] P.A.M. Basheer, Permeation analysis, in: V.S. Ramachandran, J.J. Beaudouin (Eds.) Handbook of

747 analytical techniques in concrete science and technlogy, Noyes Publications, Park Ridge, New Jersey,

748 U.S.A., 2001, pp. 658-737.

749 [62] W. Klemm, Ettringite and oxyanion-substituted ettringites - their characterization and applications in

750 the fixation of heavy metals: a synthesis of the literature, Portland Cement Association Research and

751 Development Bulletin RD116 (1998) 68p.

752 [63] Q. Zhou, F. Glasser, Kinetics and mechanism of the carbonation of ettringite, Advances in Cement

753 Research, 12 (200) 131-136.

754 [64] Y. Aono, F. Matsushita, S. Shibata, Y. Hama, Nano-structural changes of C-S-H in hardened cement

755 paste during drying at 50°C, Journal of Advanced Concrete Technology, 5 (2007) 313-323.

756 [65] X. Cong, R.J. Kirkpatrick, Effects of the temperature and relative humidity on the structure of C-S-H

757 gel, Cement and Concrete Research, 25 (1995) 1237-1245.

758 [66] E. Gallucci, X. Zhang, K. Scrivener, Effect of temperature on the microstructure of calcium silicate

759 hydrate (C-S-H), Cement and Concrete Research, 53 (2013) 185-195.

760 [67] K.S.W. Sing, E. D.S., R.A.W. Haul, L. Moscou, R.A. Pierotti, J. Rouquérol, T. Siemieniewska, Reporting

761 physisorption data for gas/solid systems with special reference to the determination of surface area and

762 porosity (Recommendations 1984), Pure and Applied Chemistry, 57 (1985) 603-619.

763 [68] E. Palou, A. López-Malo, A. Argaiz, Effect of temperature on the moisture sorption isotherms of

764 some cookies and corn snacks, Journal of Food Engineering, 31 (1997) 85-93.

765 [69] M.M. Vivanco, O.M. Taboada, Thermodynamic behavior of fish meal during adsorption, Drying

766 Technology, 16 (1998) 1827-1842.

767 [70] I.I. Salame, T.J. Bandosz, Experimental study of water adsorption on activated carbons, Langmuir, 15

768 (1999) 587-593.

769 [71] I.I. Salame, T.J. Bandosz, Study of water adsorption on activated carbons with different degrees of

770 surface oxidation, Journal of Colloid and Interface Science, 210 (1999) 367-374.

771 [72] M. Das, S. Das, Analysis of moisture sorption characteristics of fish protein myosin, International

772 Journal of Food Science and Technology, 37 (2002) 223-227.

773 [73] N. Hamdami, J.-Y. Monteau, A. Le Bail, Transport properties of a high porosity model food at above

774 and sub-freezing temperatures. Part 1: thermophysical properties and water activity, Journal of Food

775 Engineering, 62 (2004) 373-383.

776 [74] S. Timoumi, F. Zagrouba, D. Mihoubi, M.M. Tlili, Experimental study and modelling of water

777 sorption/desorption isotherms on two agricultural products: apple and carrot, Journal de Physique IV,

778 122 (2004) 235-240.

779 [75] E. Quirijns, A. van Boxtel, W. van Loon, G. van Straten, Sorption isotherms, GAB parameters and

780 isosteric heat of sorption, Journal of the Science of Food and Agriculture, 85 (2005) 1805-1814.

781 [76] C. Pérez-Alonso, C.I. Beristain, C. Lobato-Calleros, M.E. Rodríguez-Huezo, E.J. Vernon-Carter,

782 Thermodynamic analysis of the sorption isotherms of pure and blended carbohydrate polymers, Journal

783 of Food Engineering, 77 (2006) 753-760.

784 [77] R. Feldman, P. Sereda, A model for hydrated Portland cement paste as deduced from sorption-

785 length change and mechanical properties, Materials and Structures, 1 (1968) 509-520.

786 [78] H.M. Jennings, Refinements to colloid model of C-S-H in cement: CM-II, Cement and Concrete

787 Research, 38 (2008) 275-289.

788